PCCP

Electron-stimulated reactions in nanoscale water films adsorbed on α-Al_2O_3(0001)

Journal:	*Physical Chemistry Chemical Physics*
Manuscript ID	CP-ART-02-2018-001284.R1
Article Type:	Paper
Date Submitted by the Author:	06-Apr-2018

Complete List of Authors:	Petrik, Nikolay; Pacific Northwest National Laboratory, Physical Sciences Division, MSIN K8-88 P.O. Box 999 Kimmel, Greg; Pacific Northwest National Laboratory, Physical Sciences Division

SCHOLARONE™
Manuscripts

Electron-stimulated reactions in nanoscale water films adsorbed on α-Al_2O_3(0001)

Nikolay G. Petrik* and Greg A. Kimmel*

Physical Sciences Division, Pacific Northwest National Laboratory, MSIN K8-88, P.O. Box 999, Richland, WA 99352, USA.

*Corresponding authors. Email addresses – nikolai.petrik@pnnl.gov; gregory.kimmel@pnnl.gov

Abstract

The radiation-induced decomposition and desorption of nanoscale amorphous solid water (D_2O) films adsorbed on an α-Al_2O_3(0001) surface was studied at low temperature in ultrahigh vacuum using temperature programmed desorption (TPD) and electron stimulated desorption (ESD) with a mono-energetic, low energy electron source. ESD yields of molecular products (D_2, O_2 and D_2O) and the total sputtering yield increased with increasing D_2O coverage up to ~15 water monolayers (i.e. ~15 × 10^{15} cm^{-2}) to a coverage-independent level for thicker water films. Experiments with isotopically-layered water films (D_2O and H_2O) demonstrated that the highest water decomposition yields occurred at the interfaces of the nanoscale water films with the alumina substrate and vacuum. However, the increased reactivity of the water/alumina interface is relatively small compared to the enhancements in the non-thermal reactions previously observed at the water/Pt(111) and water/TiO_2(110) interfaces. We propose that the relatively low activity of Al_2O_3(0001) for the radiation-induced production of molecular hydrogen is associated with lower reactivity of this surface with hydrogen atoms, which are likely precursors for the formation of molecular hydrogen.

Keywords: water, alumina, non-thermal chemistry, nuclear waste, hydrogen, electron-stimulated desorption

I. Introduction

Aluminum is a common nuclear material and aluminum oxy-hydroxides are among the major components in highly radioactive waste. This waste is extremely complex, containing heterogeneous mixtures in highly alkaline brines that have been aging for decades in the presence of ionizing radiation.[1, 2] After long storage times, radiation affects all the components of nuclear waste: liquid, solid and interfaces. Radiation-induced processes in aqueous slurries of aluminum oxides and oxy-hydroxides are not well-understood on a fundamental level, but are potentially important for safe storage and processing of nuclear waste. Photo- and radiation-induced processes in water and aqueous systems are also important in astrochemistry and planetary sciences,[3-16] radiation- and photo-catalysis,[17-20] and radiation biology.[21-26]

High-energy radiation (α, β, γ) interacts with solids and liquids generating cascades of low-energy electrons, the most abundant of which have energies below 70 eV,[27] and these low-energy electrons are primarily responsible for most of the radiation-induced chemical transformations.[10, 27-29] Radiolysis at interfaces (e.g. oxide/water interfaces) is more complicated than the radiolysis in the individual phases (solid or liquid) since radiation absorbed in either phase can stimulate reactions at the interface producing new molecular species or surface defects. Such interfacial energy transfer was observed under gamma irradiation of water adsorbed on oxide surfaces where electronic excitations produced in the oxide can migrate to the surface and decompose water.[30-35] Depending on the substrate and water coverage, dramatic increase in the molecular hydrogen yield – up to 1 or 2 orders of magnitude compared to the radiolysis of bulk water – have been observed. Studies of gamma radiolysis of water adsorbed on Al_2O_3 powders show controversial results on substrate effect on the H_2 yield: from very small[33] to significant[30, 31, 34] enhancement.

While energy transfer from the solid to the solid/water interface can drive reactions there, radiation energy absorbed in the water can also migrate to the interface and cause enhanced water decomposition and hydrogen production there. Such an effect was previously observed in nanoscale water films adsorbed on Pt(111) and rutile TiO_2(110) that were irradiated with low-energy electrons.[36-42] For those experiments, migration of water excitons and/or hydronium ions through the condensed water to the

substrate was believed to cause the enhanced hydrogen production at the substrate interfaces.[41, 42] However, the relative efficiencies of Pt(111) and TiO_2(110) for promoting those reactions were quite different. To develop a better understanding of those electron-stimulated reactions, the role of the substrate in them, and possible connections with the gamma radiolysis experiments on oxides described above, it is useful to investigate the electron-stimulated reactions at a water/oxide interface.

Here we investigate the electron-stimulated reactions in water films deposited on α-Al_2O_3(0001). We use 100 eV electrons, which are characteristic of the low-energy secondary electrons produced by high-energy radiation (α, β, γ), as a radiation source. These electrons have short mean-free paths and therefore the experiments are performed in ultrahigh vacuum at low temperatures with solid forms of water – amorphous solid water (ASW) – as model systems for liquid water. We find that the total sputtering yield for irradiated D_2O films, measured with temperature programmed desorption (TPD), as well as the electron-stimulated desorption (ESD) yields of D_2O, D_2 and O_2 all increase with increasing water coverage, θ, in the 0 – 15 monolayers (ML) range and remain largely coverage independent above that. (Here we define 1 ML as 10^{15} cm^{-2}.) For $\theta \geq 15$ ML, the total sputtering yield is approximately 1 molecule per incident electron (with initial energy = 100 eV). Experiments with isotopically-layered D_2O/H_2O films show that the molecular hydrogen yields are greatest at the ASW/vacuum and Al_2O_3/ASW interfaces and that they are relatively low in the middle of the film. Molecular hydrogen evolution at the Al_2O_3/ASW interface is consistent with a 2-step reaction that probably includes accumulation of a precursor at the interface followed by a second reaction to produce D_2 (H_2). The electron-stimulated reactions observed in nanoscale water films on alumina are qualitatively similar to those previously observed on Pt(111) and TiO_2(110). However, much less molecular hydrogen is produced at the water/Al_2O_3(0001) interface compared to those previous experiments. Transfer of electronic excitations from the Al_2O_3 to the interface does not appear to play a significant role in the electron-stimulated reactions occurring at that interface.

II. Experimental Procedure

The experiments were carried out in an ultrahigh vacuum (UHV) system similar to that has been described previously.[37, 43] The system is equipped with a molecular beam line for dosing water and other adsorbates on the sample, a closed-cycle helium cryostat for sample cooling, a low-energy electron gun (Kimball Physics, model ELG-2), and a quadrupole mass spectrometer (Extrel, model EXM720). This system was upgraded with a Fourier-transform infrared (FTIR) spectrometer (Bruker, Vertex 80) for infrared reflection absorption spectroscopy (IRAS) performed in external reflection mode. The typical base pressure for the system was 1×10^{-10} Torr.

The 10×10×1 mm α-Al_2O_3(0001) (<0.5°) single crystal from the Princeton Scientific was mounted on resistively heated tantalum base plate using high-temperature Aremco 865 cement adhesive and a Mo retaining ring (see Fig. S1a). For temperature monitoring and control, a K-type thermocouple was spot-welded to the base plate. The Al_2O_3(0001) sample surface was prepared by sputtering with 2 keV Ne^+ ions and then annealed for 2 - 10 min in vacuum at 1050 K. Previous research has shown that this procedure produces an aluminum-terminated surface.[44-46] Thin water films were deposited with a molecular beam (flux ~2×10^{14} molecules/cm^{2}s) at normal incidence to the surface.

During ESD experiments, the electron beam was incident at 40° with respect to the sample normal. The incident energy of the electrons, E_i, used to irradiate the films was typically 100 eV, and the instantaneous current densities were ~1.8×10^{15} cm^{-2}s^{-1} as measured with a Faraday cup. The electron beam was smaller than the molecular beam spot size on the sample (~1.5 mm and 7.0 mm, respectively). To produce a uniform electron fluence across the films, the electron beam was rastered over the area slightly larger than the water spot (Fig. S1), delivering 1.5×10^{13} cm^{-2} electrons per each 0.4 s scan. The ESD signals presented below are an average of all data points in each scan (Fig. S1b). Energetic electrons that scattered from the alumina surface and subsequently irradiate other surfaces within the UHV chamber produce a measureable, "background" H_2 and HD signal in the quadrupole mass spectrometer. Therefore to investigate the production of molecular hydrogen in irradiated ASW films, we use amorphous D_2O

films (sometimes with co-adsorbed H_2O films) and track the ESD of D_2. Control experiments (see Fig. S2) show that the contribution of these background signals is small for D_2.The irradiation temperature was 100 K for all the results presented here.

III. Results and Discussion

We observed three molecular products desorbing from the D_2O ASW films grown on $Al_2O_3(0001)$ under 100 eV electron irradiation: D_2O, D_2 and O_2. Fig. 1 shows the normalized ESD yields of those products versus the irradiation time (and electron fluence, ϕ_e) for 50 ML D_2O films. The irradiation starts at 0 s and ends at 100 s. For D_2 and D_2O, the ESD signals increase promptly at the beginning of irradiation and then, after some modest changes within the first ~ 20 s, the signals remain constant. The O_2 ESD signal is zero at the beginning of irradiation, it grows with the irradiation time and then remains constant (also after ~20 s). This type of the O_2 ESD kinetics has been observed before[37, 38, 47, 48] and results from a complex, precursor-mediated mechanism for O_2 production involving OH, H_2O_2 and HO_2 intermediates (or their deuterated analogues for D_2O).[38] The ESD yields of D_2O, D_2 and O_2 increase with the initial coverage, θ_i, and their kinetic profiles also depend on the coverage (Fig. S3). For coverages smaller than shown in Fig. 1, the ESD yields do not remain constant after the initial transient period, but decrease with increasing electron fluence. The decreasing ESD yields are primarily related to the decreasing amount of water in the films as it desorbs and decomposes under irradiation.[40] For example, Fig. 2 shows a series of D_2O temperature programmed desorption (TPD) spectra for electron-irradiated films with θ_i = 1.5 ML. The TPD spectra obtained after electron irradiation demonstrate the significant loss of water due to the electron-stimulated reactions. For these experiments, almost the entire film had desorbed or reacted for $\phi_e \geq 3 \times 10^{16}$ cm^{-2}.

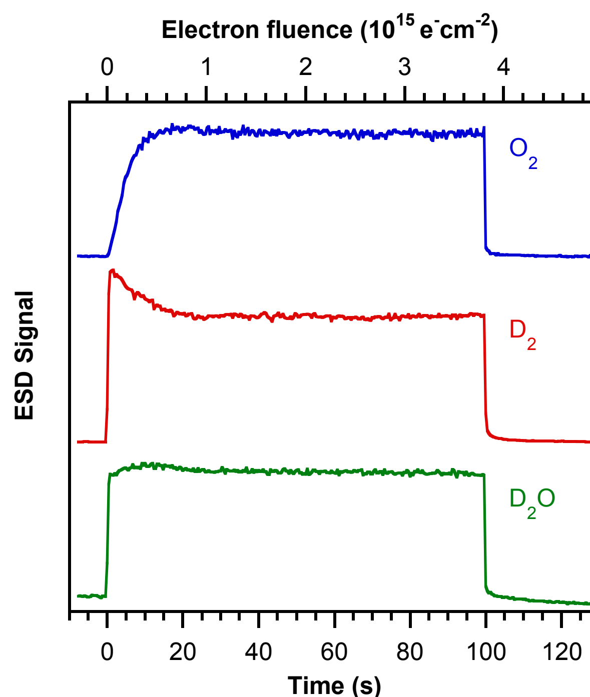

Fig. 1. D_2O, D_2 and O_2 ESD signals at 100 K versus time (bottom axis) or electron fluence (top axis) from 50 ML D_2O films on $Al_2O_3(0001)$. (1 ML = 10^{15} cm^{-2}). The signals are normalized and displaced for the sake of comparison. Irradiation starts at 0 s and ends at 100 s.

For sufficiently thick water films, the fact than the ESD signals remain constant over the longer irradiation times (see Fig. 1) indicates that charging of such a wide band gap dielectric like alumina is not a critical issue here, otherwise the incident electrons would not be able to reach the charged sample and the ESD signals would decrease to zero with time. Instead, the system achieves a steady state configuration in which the incident electron flux is balanced by the flux of secondary and scattered electrons leaving the surface.[49] Because many of the secondary electrons have very low energies, small amounts of charging (either positive or negative) can change their escape probability allowing the steady state to be achieved and maintained. ESD of charged atoms, molecules and clusters[50-57] will also influence the charge balance, but contribution of these species are small relative to the electrons.

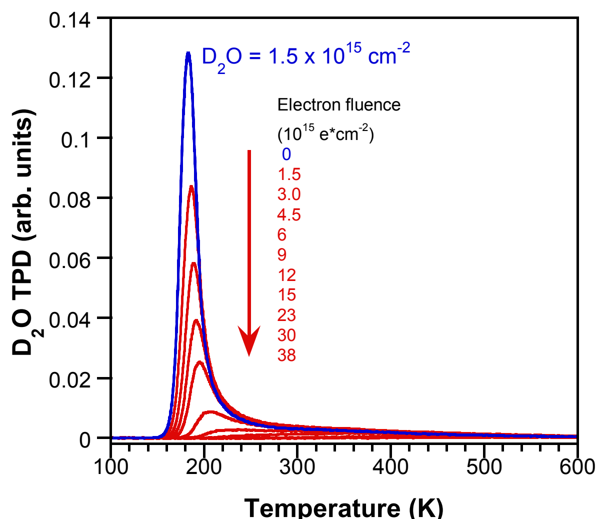

Fig. 2. Post-irradiation D_2O TPDs versus the irradiation dose at 100 K. $\theta(D_2O) = 1.5$ ML ~ 1.5×10^{15} cm^{-2}

Integrated D_2O, D_2 and O_2 ESD yields versus θ_i are shown in Fig. 3 (green, red and blue circles, respectively). The integrated ESD yields are obtained from the data such as those shown in Fig. 1 and S2 integrated over range $0 \leq \phi_e \leq 3.8 \times 10^{15}$ cm^{-2}. For $\theta_i < 3$ ML, the ESD yields of the molecular products increase monotonically versus the initial D_2O coverage (Fig. 3a). A one monolayer water film is sufficiently thin that most of the electronic excitations produced by the incident electrons occur in the Al_2O_3 substrate, and these excitations could potentially contribute to the non-thermal reactions in the adsorbed water via interfacial energy transfer. Such energy transfer proceeds primarily between the substrate and the first molecular layer of water in direct contact with it, and has been observed for numerous metal oxides irradiated with gamma rays and other high-energy radiation.[30, 31, 33, 58, 59] However, the data in Fig. 3a show that there is no enhancement of the ESD yields for the first water monolayer as compared to the second and the third ones, which suggests that any additional water radiolysis due to the energy transmitted from the Al_2O_3 substrate is limited in these experiments. The current observations agrees with some of the previous works reporting relatively low catalytic activity for alumina in gamma radiolysis of the adsorbed water.[33]

Integrated D_2O, D_2 and O_2 ESD yields for higher coverages of D_2O on $Al_2O_3(0001)$ are presented in Fig. 3b. The ESD yields are normalized by their maximum signals and displaced for the sake of comparison. Fig. 3b also shows the total sputtering yield, $\Delta\theta = \theta_i - \theta(\phi_e)$, for irradiated films with $\phi_e = 1.5 \times 10^{15}$ cm^{-2} (grey diamonds). $\theta(\phi_e)$, which is the amount of water remaining in a film after electron irradiation, is calculated from the integral of the water TPD spectra after irradiation (see Fig. 2). The ESD yields increase with water coverage up to ~ 15 ML (which corresponds to a film thickness of ~ 5 nm) and then remain largely constant (Fig. 3b). [60] The total sputtering yield is a measure of all the water degradation channels, including the ESD of neutral D_2O, molecular reaction products (e.g. D_2 and O_2), radicals D, O, OD,[38, 61-64] and various positive and negative ionic species.[51-53, 56, 57] The reactions yielding molecular products (D_2O, D_2 and O_2) are believed to make the largest contribution to the total sputtering yield.[40]

Qualitatively similar results for the integrated D_2O, D_2 and O_2 ESD yield versus coverage were observed previously for ASW films deposited on Pt(111)[40] and rutile $TiO_2(110)$.[37] In those earlier studies, several factors contributed to the coverage-dependent ESD yields including the total number and spatial distribution of the initial ionizations and electronic excitations produced by the incident electrons in the ASW films and the spatial distribution of the resulting non-thermal reactions (which due to the mobility of the excited species in ASW is distinct from the initial distribution).[39-42] For $Al_2O_3(0001)$, both the D_2 and O_2 ESD yields have small maxima at θ_i ~ 12 ML (Fig. 3b). Similar maxima were observed for Pt(111) and $TiO_2(110)$ substrates, but the maxima were more pronounced. The earlier studies demonstrated that the maxima in the ESD yields are related to non-thermal reactions at the water/substrate interface.[37, 39-42] Therefore, the smaller maxima observed in the D_2 and O_2 ESD yields on $Al_2O_3(0001)$ suggest that this surface is less reactive than either Pt(111) or $TiO_2(110)$. Because the O_2 and (one component of the) D_2 are produced in multi-step reactions that require the creation of precursors before significant amounts of the final product are produced, the detailed shapes of the integrated D_2 and O_2 yields versus θ_i depend somewhat on the integration range that is chosen for the electron fluences (see

Fig. S4). The reactions occurring at the water/Al_2O_3(0001) interface will be discussed in more detail below.

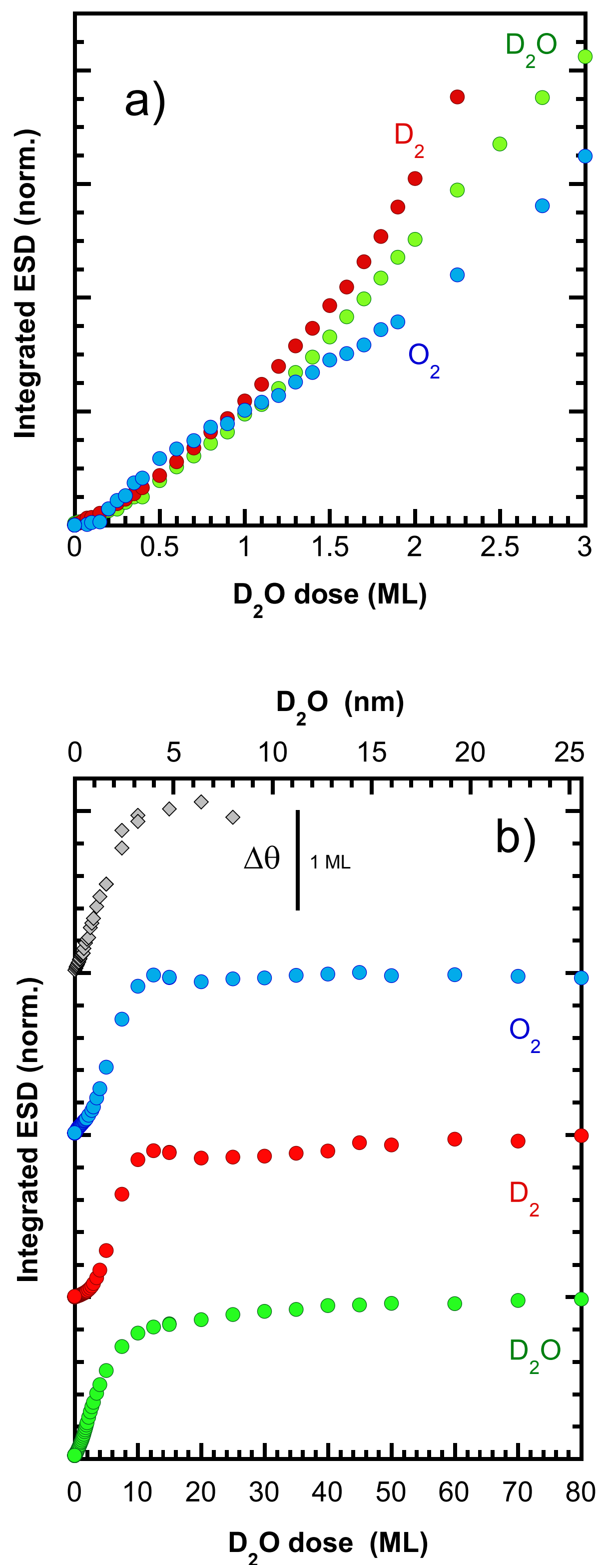

Fig. 3. Integrated D_2O, D_2 and O_2 ESD yields (green, red and blue filled circles, respectively) and the total sputtering yield ($\Delta\theta$) from TPD measurements (gray filled diamonds) versus initial D_2O coverage, θ_i, on $Al_2O_3(0001)$. The integrated ESD yields are calculated for $\phi_e = 3.8 \times 10^{15}$ cm^{-2}. The sputtering yield was measured for $\phi_e = 1.5 \times 10^{15}$ cm^{-2}. Note: due to sputtering, actual film coverage by the end of irradiation is smaller than the initial one. All yields are normalized by the maximum yield and displaced (in panel (b)) for the sake of comparison.

For $\phi_e = 1.5 \times 10^{15}$ cm^{-2} and θ_i ~15 ML, the total amount of sputtered water is ~ 1.7 ML, which corresponds to a total sputtering yield of ~ 1.1 molecules/electron. Since the energy of the electrons is 100 eV, the radiation chemical yield (G-value) for the number of D_2O molecules removed per 100 eV of absorbed energy would be G(-D_2O) ~ 1.1 molecules/100 eV. This yield is comparable with reported yields of total water decomposition under gamma irradiation of ice: 1.0 and 0.5 molecules/100 eV at 195 and 73 K respectively.[65] In our earlier studies for thin D_2O films on Pt(111) surface, the total sputtering yield was ~ 1.7 molecules/electron (for 87 eV electrons and 27 ML D_2O).[40]

Isotopically-layered water films are useful for studying the spatial distribution of radiation-chemical reactions in nanoscale ASW films on substrates.[5, 36-39, 41, 42, 66, 67] Fig. 4 shows the integrated D_2 ESD yield for "sandwich" $H_2O/D_2O/H_2O$ films grown at 100 K in which a thin 3 ML D_2O layer is deposited at different positions within a 28 ML H_2O film. In this experiment, the position of the D_2O layer is varied from the ASW/$Al_2O_3(0001)$ interface to the ASW/vacuum interface (see schematic, Fig. 4). The integrated D_2 ESD yield is the smallest when the D_2O layer is placed inside the H_2O film and it increases when the D_2O layer is located at either interface: ~ 4 times at the ASW/$Al_2O_3(0001)$ interface and ~ 40 times at ASW/vacuum interface (Fig. 4). Qualitatively similar results were reported for the isotopically layered ASW films on Pt(111)[41] and $TiO_2(110)$.[37] Because the structure of the ASW/vacuum interface should not depend on the substrate for water films with coverages of ~ 30 ML, the D_2 ESD yield at that interface should also not depend on the substrate. Therefore, the ratio of the D_2 ESD yields at the ASW/substrate and ASW/vacuum interface for various substrates, φ(sub), provides a measure of the relative efficiency of the substrates in promoting non-thermal reactions. For similar experiments with

layered $H_2O/D_2O/H_2O$ films on Pt(111),[41] $TiO_2(110)$,[37] and $Al_2O_3(0001)$ (Fig. 4a) we find $\varphi(Pt(111)) = 2.4$, $\varphi(TiO_2(110)) = 0.34$, and $\varphi(Al_2O_3(0001)) = 0.10$, indicating that $Al_2O_3(0001)$ is the least reactive of these three substrates for hydrogen production.

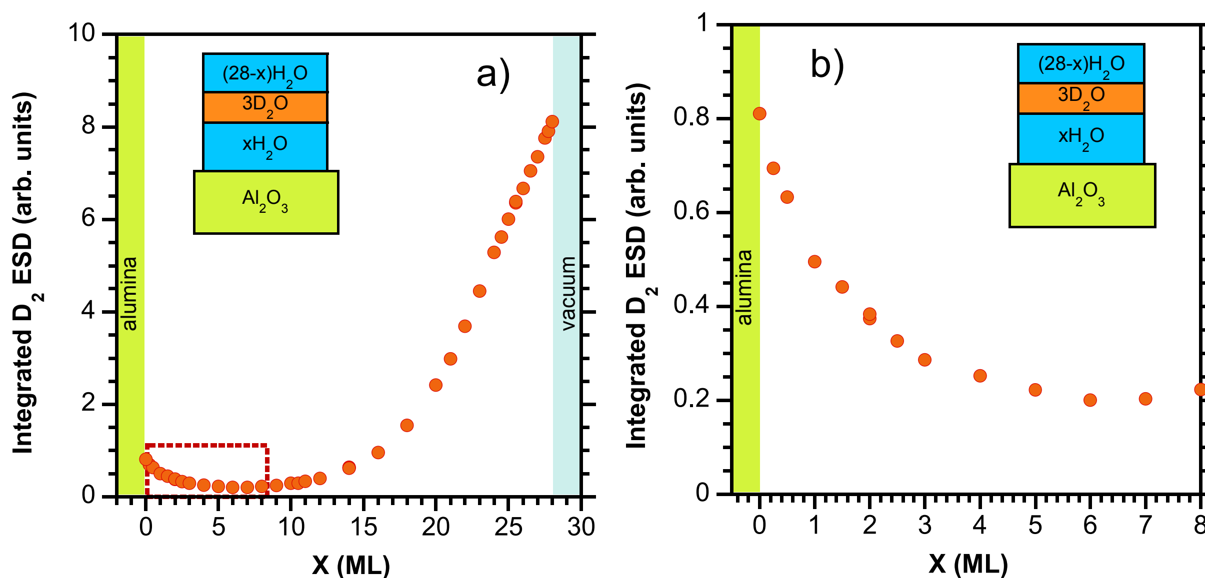

Fig. 4. Integrated D_2 ESD yield from layered $H_2O/D_2O/H_2O$ films on $Al_2O_3(0001)$ versus the D_2O layer position relative to the alumina surface measured by the H_2O spacer layer coverage. D_2O thickness is 3 ML and the total H_2O coverage is 28 ML. The right panel shows zoomed area indicated in the left panel with red square.

Another experiment, in which a 3 ML D_2O layer was deposited directly on the $Al_2O_3(0001)$ and capped with various coverage of H_2O (see Fig. 5), illustrates the importance of energy transfer from the bulk of the water film to the water/$Al_2O_3(0001)$ interface for the molecular hydrogen production. Without the H_2O cap, the D_2 ESD signal increases promptly when the electron beam turned on and then it decays gradually with increasing electron fluence as the film decomposes under irradiation (Fig. 5a). As the coverage of the H_2O cap was increases, this initial ESD signal decreases exponentially with a 1/e constant of ~ 2.3 ML (Fig. 5b, red circles). According to our previous studies,[37, 41, 42] this prompt ESD component is associated mainly with D_2 produced at the ASW/vacuum interface and it decreases as the D_2O at this

interface is replaced with H_2O. On the other hand, the total integrated D_2 ESD yield from the fixed amount of D_2O (Fig. 5b, blue squares) initially increases with the H_2O cap layer coverage as more of the energy of the incident electrons is absorbed in the water film and transferred to the $D_2O/Al_2O_3(0001)$ interface where it drives the non-thermal reactions.[37, 41, 42] After reaching a maximum when the H_2O cap layer is ~9 ML, the D_2 yield decreases to very low levels with further increases in the H_2O coverage. The lower yield is related to the decreased rate of reactions at the ASW/$Al_2O_3(0001)$ interface for thicker films. The probability of electronic excitations produced within the films reaching the substrate decreases inversely proportional to the coverage,[42] leading to the lower rates there. Because the same electron fluence is used for the integrated D_2 ESD signal at all coverages, the lower reaction rate translates into a lower yield for larger coverages. However, qualitatively similar results are obtained for other electron fluences (see Fig. S5 and the supplemental information for more discussion of this issue). The maximum in the D_2 ESD yield shown in Fig. 5b and S5 is closely related to the small maximum observed in the D_2 ESD yield versus coverage for a pure D_2O film (see Fig. 3b and S4a). The maximum is more pronounced in Fig. 5b because for that experiment the coverage-dependent changes in the molecular hydrogen produced at the ASW/vacuum interface are occurring in the H_2O cap layer leading to more H_2 ESD. As discussed above, the enhanced reactivity for $Al_2O_3(0001)$ is relatively small: The maximum for the integrated D_2 ESD, normalized by the yield for the 3 ML D_2O film without any H_2O, is ~ 1.35 (Fig. 5b). In comparable experiments on Pt(111)[41] and $TiO_2(110)$,[37] the D_2 ESD yields increased up to ~12 times for $TiO_2(110)$ and up to ~18 times for Pt(111) with the increased H_2O cap layer coverage. Therefore, while both experiments with isotopically layered films (see Fig. 4 and 5) show enhancement of the molecular hydrogen production at the ASW/$Al_2O_3(0001)$ interface, the magnitude of the enhancement is significantly less than previous observed on Pt(111) and $TiO_2(110)$.

D_2 produced at the substrate/ASW interface has to diffuse through the water film to desorb. As a result, it can be detected for several seconds after the end of irradiation. This post-irradiation "outgassing," which has been observed previously for the Pt(111)/ASW system,[41, 42] was also observed for the $Al_2O_3(0001)$/ASW (Fig. S6). However due to the lower reactivity of the alumina, the "outgassing"

signal is much smaller in this case. Note also that the time needed for D_2 to diffuse from the ASW/alumina interface to the vacuum interface is not responsible for the slow increase in the D_2 ESD signal at larger H_2O coverages seen in Fig. 5a (see also Fig. 6 and the discussion below).

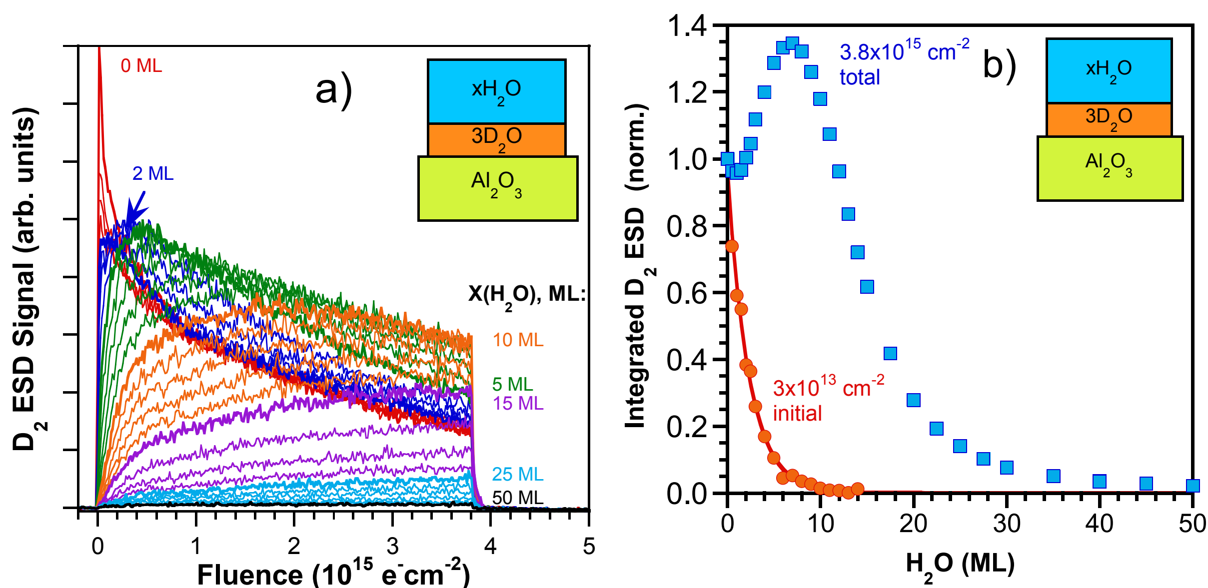

Fig. 5. a) D_2 ESD signal versus irradiation fluence from isotopically layered D_2O/H_2O films on $Al_2O_3(0001)$ versus the initial H_2O cap coverage. D_2O thickness is 3 ML and the H_2O coverage increases from 0 to 50 ML. b) Integrated D_2 ESD yield versus the H_2O cap coverage: $0 \leq \phi_e \leq 3 \times 10^{13}$ cm^{-2} (initial ESD yield, red circles) and $0 \leq \phi_e \leq 3.8 \times 10^{15}$ cm^{-2} (total ESD yield, blue squares). The data are normalized for the sake of comparison.

The D_2 ESD kinetics for the D_2O layer capped with various coverages of H_2O provide valuable insight into the reaction mechanisms (see Fig. 5a). Without the H_2O cap, non-thermal reactions at the D_2O/vacuum interface lead to the prompt increase in the D_2 ESD signal when the electron beam is turned on.[5, 6, 37, 41, 42, 47, 68] For H_2O coverages greater than a few monolayers, these reactions produce H_2 and thus do not contribute to the D_2 ESD that is observed. With an H_2O cap layer in place, the initial D_2 ESD signal is essentially zero and it increases gradually with the electron fluence. These kinetics indicate that D_2 is produced at the water/Al_2O_3 interface via a multi-step reaction sequence. The simplest model would be a two-step reaction in which the first reaction produces a precursor, *P*, and a second reaction leads to

D_2. Similar precursor-mediated kinetics for the evolution of molecular hydrogen from the buried interfaces were observed earlier for Pt(111) and TiO_2(110).[37, 41] For both those substrates, the reactions involved the accumulation of hydrogen atoms on the substrate and their recombination leading to the molecular hydrogen production. On Pt(111) and TiO_2(110), the accumulation of hydrogen atoms on those surfaces led to distinct changes in the water TPD spectra that facilitated the identification of the precursor.[37, 69] For water on Al_2O_3(0001), the water TPD spectra after electron irradiation are quite similar to the spectra for un-irradiated films (Fig. 2, S7a). We also have not seen any molecular hydrogen desorption during thermal annealing of irradiated water films. With such low activity of the alumina substrate in the hydrogen production, the concentration of the precursor "*P*" may be below our detection sensitivity and its identity is uncertain. However, experiments where a water film is irradiated twice, with a variable delay time between the irradiations, indicate that the precursor is relatively stable at 100 K (see Fig. 6). During the first irradiation, the ESD signal increases with time as the D_2 precursor builds up (Fig. 6, red line). After a 1200 s delay, the D_2 ESD signal increases rapidly to the level it had at the end of the first irradiation (Fig. 6, blue line), indicating that the D_2 precursor survived for 1200 s at 100 K. Note that the shorter rise time for the D_2 ESD in the second irradiation is associated with the time needed for the D_2 produced at the buried interface to diffuse through the H_2O cap layer prior to desorbing.

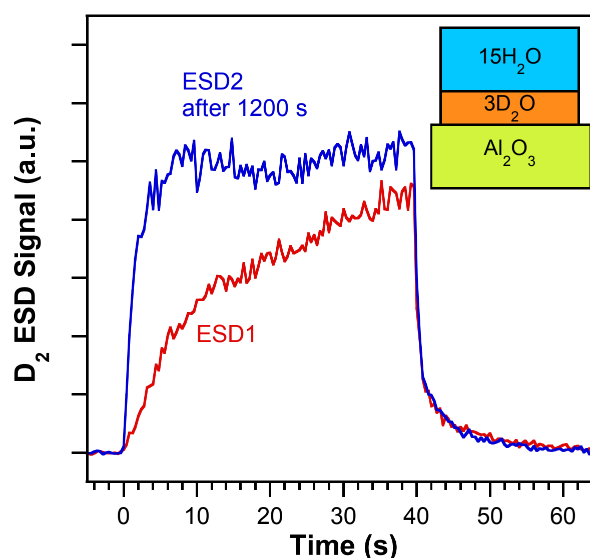

Fig. 6. D_2 ESD signals at 100 K versus time from an isotopically-layered 3 ML D_2O/15 ML H_2O film on Al_2O_3(0001). The first irradiation, ESD1, starts at 0 s and ends at 40 s (red line). A second irradiation, ESD2, starts 1200 s after the end of the first irradiation (blue line).

The experiments with isotopically-layered water films (see Figs. 4 and 5) demonstrate that the radiation-induced processes in nanoscale ASW films on Al_2O_3(0001) include three spatially resolved components associated with the water/vacuum interface, the "bulk" water, and the water/Al_2O_3 interface. The first two components are most likely independent of the substrate type[70] and their reaction mechanisms have been discussed previously.[38-42, 61, 63, 71-77] The basic idea is that the differences in the reactivity of water molecules at the vacuum interface of ASW films or within the films is associated with differences in the electronic structure and *O-H* bond dissociation dynamics of excited water molecules in those different environments.[37, 38, 78-80] In the gas phase, the first electronically-excited state of water dissociates into H + OH without any barrier.[81] However, if an OH group of a water molecule participates in a hydrogen bond, then the lowest excited state is non-dissociative and relatively long-lived.[79, 80] Therefore electronically-excited water molecules within the films are less likely to dissociate compared to excited molecules on the surface. Several observations support this hypothesis, including the observed increase in the integrated D_2O ESD yield versus θ_i (see Fig. 3b). In that case, the argument is that the electronic excitation cross section for molecular water is largely independent of its location within a water film. Therefore the direct electronic excitation of the water at the vacuum interface will not depend on the coverage. Because only water at the vacuum interface can desorb and water desorption due to simple momentum transfer from translationally-hot water molecules in the subsurface is very unlikely, this leaves mobile excitations as the most likely explanation for the increasing D_2O ESD yield versus coverage. Earlier measurements of the D atom ESD from electron-irradiated water films also show that the migration of electronic excitations to the vacuum interface is important,[63] and optical experiments and theory support the existence of excitons in condensed water.[79, 82-86]

For the electron-stimulated reactions at the interface between the water film and the substrate, the results on Pt(111), TiO_2(110) and Al_2O_3(0001) show that all these substrates increase the amount of hydrogen produced relative to the hydrogen produced in the middle of the water films, but the degree of enhancement depends on the substrate. In analogy with the effects of the vacuum interface on the excited-state dynamics, it is likely that differences in the bonding configurations of water molecules at a solid surface could also lead to differences in the non-thermal reactions. However, we are unaware of any calculations that investigate the reaction dynamics of electronically-excited water molecules at or near solid substrates. Furthermore, the substrates could also have more typical catalytic effects on the reactions that are not directly related changes in the excited state dynamics. To further discuss the results for hydrogen production at the water/alumina interface, it is useful to review the reactions steps that have been postulated in the production of molecular hydrogen at the water/platinum interface. These steps include:

1. Electronic excitation and/or ionization of water molecules by the incident electrons within their penetration depth in the water film creating mobile water excitons and/or hydronium ions.
2. Migration of water excitons and/or hydronium ions to the water/Pt substrate interface.
3. Reaction of the excitons and/or hydronium ions with the Pt substrate to produce adsorbed hydrogen atoms, H_{ads}.
4. Once the coverage of hydrogen atoms on the Pt substrate reached a certain level, H_2 is formed by reactions between adsorbed hydrogen atoms: $2H_{ads} \rightarrow H_2$ (or $2D_{ads} \rightarrow D_2$).
5. Once formed, molecular hydrogen desorbs from the Pt substrate, diffuses through the water film and desorbs if it reaches the vacuum interface.

It is important to note that the second step – migration of water excitons and/or hydronium ions – is necessary to explain the observation that H or D atoms accumulate on the surface if H_2O or D_2O comprise the water layer adjacent to the substrate, respectively. If not for this observation, water dissociation into H + OH (or D + OD) at the location of the initial electronic excitation followed by diffusion of the atom through the water film to the substrate would be the preferred explanation. For

electron-stimulated production of hydrogen at the water/TiO_2(110) interface,[37] steps 1 and 2 were probably the same or quite similar. (Note that the sample preparation used for UHV experiments on rutile TiO_2(110) results in a bulk-reduced crystal that is conducting.) Therefore, the substrate can supply electrons for step 2 without building up charge at that interface. However, because hydrogen adsorption is different on Pt(111) and TiO_2(110),[37, 87, 88] the subsequent steps were modified. In particular, the ESD experiments showed that hydrogen atoms that reacted with bridging oxygen atoms to form bridging hydroxyls were stable and did not lead to H_2. Instead, hydrogen atoms adsorbing on the Ti sites were probably the precursor for H_2 produced at that interface.

For the electron-stimulated reactions in water films adsorbed on alumina, the reactions that are most likely influenced by the substrate are reactions 3 and 4. For alumina, the net reaction to produce molecular hydrogen from hydronium ions, $2(H_3O^+ + e^-) \rightarrow 2H_2O + H_2$, would require 2 electrons from the substrate. However since alumina is an insulator, it probably cannot sustain such a reaction, in contrast to both Pt(111) and TiO_2(110). Thus, the lower reactivity of alumina could be associated with less reactions of hydronium at that buried interface.

The stability of hydrogen on the alumina surface could also be an important factor. For example, experiments investigating H-atom spillover from platinum particles onto an alumina support[89] found that H_2 desorbed at ~700 K, which was much higher than its desorption temperature from the platinum.[90, 91] Thus the reduced reactivity of the alumina surface could result from a higher binding energy for hydrogen atoms. However, if the concentration of hydrogen atoms were appreciably increasing on the surface, we would expect these to change the water TPD spectra of irradiated films. The lack of such changes (see Fig. 2, S7) argues against a significant accumulation of hydrogen on the alumina from the electron irradiation. More studies are needed to identify the chemical form of the precursor for molecular hydrogen building up on the alumina surface under irradiation.

IV. Conclusions

In summary, we have investigated low energy electron-stimulated processes in films of amorphous solid water (D_2O) deposited on the surface (0001) of single crystal α-Al_2O_3. During irradiation with 100 eV electrons at low temperature (100 K), D_2, O_2 and D_2O are produced and desorbed from the surface and their yield increase with the initial D_2O coverage up to 15 ML ($\sim 15 \times 10^{15}$ cm^{-2}), becoming coverage-independent for thicker films. Total water sputtering yield follows a similar trend reaching value of ~1.1 molecules per a 100 eV electron. D_2O/H_2O isotopic layering experiments show that most of the molecular hydrogen is produced at the interfaces of the film with vacuum and with the alumina substrate, but most of the electronic excitations driving these reactions occur in the bulk of the film. Many features of the observed electron-stimulated processes are quite similar to those previously studied for the water layers on the surface of Pt(111)[38-42] and TiO_2(110),[36] especially for the thicker films, where the substrate effects are negligible. As compared to these substrates, water decomposition and molecular hydrogen production at the Al_2O_3/ASW is significantly less efficient. We tentatively associate this with different electronic properties of alumina resulting in lower reactivity with the radiation-produced hydrogen atoms – possible precursors for the molecular hydrogen.

Conflicts of interest

There are no conflicts to declare

Acknowledgements:

This work was supported as part of IDREAM (Interfacial Dynamics in Radioactive Environments and Materials), an Energy Frontier Research Center funded by the U.S. Department of Energy (DOE), Office of Science, Basic Energy Sciences. Pacific Northwest National Laboratory (PNNL) is a multiprogram national laboratory operated for the U.S. Department of Energy by Battelle Memorial Institute under Contract No. DE-AC05-76RL01830. The research was performed using the

Environmental Molecular Sciences Laboratory, a national scientific user facility sponsored by the Department of Energy's Office of Biological and Environmental Research and located at PNNL.

Supplementary Information

Electronic Supplementary Information (ESI) available: Fig. S1, Secondary electron and ESD images of water films deposited on the $Al_2O_3(0001)$ sample; Fig. S2 and S3, D_2O, D_2 and O_2 ESD signals versus electron fluence from various coverages of D_2O; Fig. S4 and S5, D_2, O_2, and D_2O ESD yields integrated in different electron fluence ranges; Fig. S6, D_2 signal measured after irradiation versus D_2O coverage; Fig. S7, D_2O TPD from the irradiated samples.

References

1. J. G. Reynolds, J. K. McCoskey and D. L. Herting, *Ind. Eng. Chem. Res.*, 2016, **55**, 5465-5473.
2. R. A. Peterson, E. C. Buck, J. Chun, R. C. Daniel, D. L. Herting, E. S. Ilton, G. J. Lumetta and S. B. Clark, *Environmental Science & Technology*, 2018, **52**, 381-396.
3. T. Hama and N. Watanabe, *Chem. Rev.*, 2013, **113**, 8783-8839.
4. N. Watanabe and A. Kouchi, *Prog. Surf. Sci.*, 2008, **83**, 439-489.
5. K. A. K. Gadallah, D. Marchione, S. P. K. Koehler and M. R. S. McCoustra, *Phys. Chem. Chem. Phys.*, 2017, **19**, 3349-3357.
6. A. G. M. Abdulgalil, A. Rosu-Finsen, D. Marchione, J. D. Thrower, M. P. Collings and M. R. S. McCoustra, *ACS Earth Space Chem.*, 2017, **1**, 209-215.
7. D. Marchione and M. R. S. McCoustra, *Phys. Chem. Chem. Phys.*, 2016, **18**, 29747-29755.
8. R. E. Johnson, in *Physics and Chemistry at Low Temperatures*, ed. L. Khriachtchev, Pan Stanford Publishing Singapore, 2011, pp. 297 - 339.

9. T. Cassidy, P. Coll, F. Raulin, R. W. Carlson, R. E. Johnson, M. J. Loeffler, K. P. Hand and R. A. Baragiola, *Space Sci. Rev.*, 2010, **153**, 299-315.

10. B. C. Garrett, D. A. Dixon, D. M. Camaioni, D. M. Chipman, M. A. Johnson, C. D. Jonah, G. A. Kimmel, J. H. Miller, T. N. Rescigno, P. J. Rossky, S. S. Xantheas, S. D. Colson, A. H. Laufer, D. Ray, P. F. Barbara, D. M. Bartels, K. H. Becker, H. Bowen, S. E. Bradforth, I. Carmichael, J. V. Coe, L. R. Corrales, J. P. Cowin, M. Dupuis, K. B. Eisenthal, J. A. Franz, M. S. Gutowski, K. D. Jordan, B. D. Kay, J. A. LaVerne, S. V. Lymar, T. E. Madey, C. W. McCurdy, D. Meisel, S. Mukamel, A. R. Nilsson, T. M. Orlando, N. G. Petrik, S. M. Pimblott, J. R. Rustad, G. K. Schenter, S. J. Singer, A. Tokmakoff, L. S. Wang, C. Wittig and T. S. Zwier, *Chem. Rev.*, 2005, **105**, 355-389.

11. T. E. Madey, R. E. Johnson and T. M. Orlando, *Surf. Sci.*, 2002, **500**, 838-858.

12. R. A. Baragiola, *Planet Space Sci.*, 2003, **51**, 953-961.

13. D. A. Bahr, M. Fama, R. A. Vidal and R. A. Baragiola, *J. Geophys. Res.-Planets*, 2001, **106**, 33285-33290.

14. T. M. Orlando, T. B. McCord and G. A. Grieves, *Icarus*, 2005, **177**, 528-533.

15. X. N. Pan, A. D. Bass, J. P. Jay-Gerin and L. Sanche, *Icarus*, 2004, **172**, 521-525.

16. T. B. McCord, T. M. Orlando, G. Teeter, G. B. Hansen, M. T. Sieger, N. G. Petrik and L. Van Keulen, *J. Geophys. Res.-Planets*, 2001, **106**, 3311-3319.

17. A. Fujishima, X. T. Zhang and D. A. Tryk, *Surf. Sci. Rep.*, 2008, **63**, 515-582.

18. G. A. Zacheis, K. A. Gray and P. V. Kamat, *J. Phys. Chem. B*, 1999, **103**, 2142-2150.

19. J. Belloni, *Catal. Today*, 2006, **113**, 141-156.

20. A. G. Okunev and Y. I. Aristov, *React. Kinet. Catal. Lett.*, 1996, **58**, 349-357.

21. K. Kobayashi, in *Charged Particles and Photon Interactions with Matter*, eds. A. Mozumder and Y. Hatano, Marcel Dekker, New York - Basel, 2004, pp. 471 - 489.

22. W. F. Morgan and W. J. Bair, *Radiat. Res.*, 2013, **179**, 501-510.

23. W. A. Bernhard and D. M. Close, in *Charged Particles and Photon Interactions with Matter*, eds. A. Mozumder and Y. Hatano, Marcel Dekker, New York - Basel, 2004, pp. 431 - 470.

24. X. Pan and L. Sanche, *Phys. Rev. Lett.*, 2005, **94**.

25. F. Martin, P. D. Burrow, Z. L. Cai, P. Cloutier, D. Hunting and L. Sanche, *Phys. Rev. Lett.*, 2004, **93**.

26. B. Boudaiffa, P. Cloutier, D. Hunting, M. A. Huels and L. Sanche, *Science*, 2000, **287**, 1658-1660.

27. A. D. Bass and L. Sanche, in *Charged Particles and Photon Interactions with Matter*, eds. A. Mozumder and Y. Hatano, Marcel Dekker, New York - Basel, 2004, pp. 207 - 257.

28. C. R. Arumainayagam, H. L. Lee, R. B. Nelson, D. R. Haines and R. P. Gunawardane, *Surf. Sci. Rep.*, 2010, **65**, 1-44.

29. M. C. Boyer, N. Rivas, A. A. Tran, C. A. Verish and C. R. Arumainayagam, *Surf. Sci.*, 2016, **652**, 26-32.

30. S. C. Reiff and J. A. LaVerne, *Radiat. Phys. Chem.*, 2017, **131**, 46-50.

31. A. A. Garibov, T. N. Agaev, S. Z. Melikova, G. T. Imanova and I. A. Faradjzade, *Nanotechnol. Russia*, 2017, **12**, 252 - 257.

32. S. Le Caer, *Water*, 2011, **3**, 235-253.

33. N. G. Petrik, A. B. Alexandrov and A. I. Vall, *J. Phys. Chem. B*, 2001, **105**, 5935-5944.

34. A. A. Garibov, M. M. Melikzade, M. Y. Bakirov and M. K. Ramazanova, *High Energy Chem.*, 1982, **16**, 177-179.

35. O. Roth, B. Dahlgren and J. A. LaVerne, *J. Phys. Chem. C*, 2012, **116**, 17619-17624.

36. R. S. Smith, N. G. Petrik, G. A. Kimmel and B. D. Kay, *Accounts of Chemical Research*, 2012, **45**, 33-42.

37. N. G. Petrik and G. A. Kimmel, *J. Phys. Chem. C*, 2009, **113**, 4451-4460.

38. N. G. Petrik, A. G. Kavetsky and G. A. Kimmel, *J. Phys. Chem. B*, 2006, **110**, 2723-2731.

39. N. G. Petrik, A. G. Kavetsky and G. A. Kimmel, *J. Chem. Phys.*, 2006, **125**, 124702.

40. N. G. Petrik and G. A. Kimmel, *J. Chem. Phys.*, 2005, **123**, 054702.

41. N. G. Petrik and G. A. Kimmel, *J. Chem. Phys.*, 2004, **121**, 3736 - 3744.

42. N. G. Petrik and G. A. Kimmel, *Phys. Rev. Lett.*, 2003, **90**, 166102.

43. C. D. Lane, N. G. Petrik, T. M. Orlando and G. A. Kimmel, *J. Phys. Chem. C*, 2007, **111**, 16319-16329.

44. H. Kirsch, J. Wirth, Y. Tong, M. Wolf, P. Saalfrank and R. K. Campen, *J. Phys. Chem. C*, 2014, **118**, 13623-13630.

45. J. Ahn and J. W. Rabalais, *Surf. Sci.*, 1997, **388**, 121-131.

46. Y. Tong, J. Wirth, H. Kirsch, M. Wolf, P. Saalfrank and R. K. Campen, *J. Chem. Phys.*, 2015, **142**, 054704.

47. C. T. Reimann, J. W. Boring, R. E. Johnson, J. W. Garrett, K. R. Farmer, W. L. Brown, K. J. Marcantonio and W. M. Augustyniak, *Surf. Sci.*, 1984, **147**, 227-240.

48. M. T. Sieger, W. C. Simpson and T. M. Orlando, *Nature*, 1998, **394**, 554-556.

49. Y. Horowitz and M. Asscher, *J. Chem. Phys.*, 2012, **136**, 134701.

50. P. Rowntree, L. Parenteau and L. Sanche, *J. Chem. Phys.*, 1991, **94**, 8570-8576.

51. W. C. Simpson, L. Parenteau, R. S. Smith, L. Sanche and T. M. Orlando, *Surf. Sci.*, 1997, **390**, 86-91.

52. W. C. Simpson, M. T. Sieger, T. M. Orlando, L. Parenteau, K. Nagesha and L. Sanche, *J. Chem. Phys.*, 1997, **107**, 8668-8677.

53. M. T. Sieger, W. C. Simpson and T. M. Orlando, *Phys. Rev. B*, 1997, **56**, 4925-4937.

54. M. T. Sieger and T. M. Orlando, *Surf. Sci.*, 2000, **451**, 97-101.

55. T. M. Orlando, A. B. Aleksandrov and J. Herring, *J. Phys. Chem. B*, 2003, **107**, 9370-9376.

56. J. Herring-Captain, G. A. Grieves, A. Alexandrov, M. T. Sieger, H. Chen and T. M. Orlando, *Phys. Rev. B*, 2005, **72**.

57. J. Herring, A. Aleksandrov and T. M. Orlando, *Phys. Rev. Lett.*, 2004, **92**.

58. J. A. LaVerne, *J. Phys. Chem. B*, 2005, **109**, 5395-5397.

59. J. A. LaVerne and L. Tandon, *J. Phys. Chem. B*, 2002, **106**, 380-386.

60. For films thicker than ~40 ML, small changes in the detection sensitivity of the QMS from experiment to experiment make it difficult to accurately measure small changes in coverage from sputtering. As a result, the displayed sputtering data is limited to $\theta < 25$ ML.

61. G. A. Kimmel and T. M. Orlando, *Phys. Rev. Lett.*, 1995, **75**, 2606-2609.

62. G. A. Kimmel, T. M. Orlando, P. Cloutier and L. Sanche, *J. Phys. Chem. B*, 1997, **101**, 6301-6303.

63. T. M. Orlando and G. A. Kimmel, *Surf. Sci.*, 1997, **390**, 79-85.

64. M. C. Akin, N. G. Petrik and G. A. Kimmel, *J. Chem. Phys.*, 2009, **130**, 104710.

65. C. J. Hochanadel, ed., *Radiation chemistry of water*, New York, Wiley, San Juan, 1960.

66. N. G. Petrik and G. A. Kimmel, *J. Phys. Chem. B*, 2005, **109**, 15835-15841.

67. N. G. Petrik, R. J. Monckton, S. P. K. Koehler and G. A. Kimmel, *J. Chem. Phys.*, 2014, **140**, 204710.

68. G. A. Kimmel, R. G. Tonkyn and T. M. Orlando, *Nucl. Instrum. Meth. B*, 1995, **101**, 179-183.

69. N. G. Petrik and G. A. Kimmel, *J. Chem. Phys.*, 2004, **121**, 3727 - 3735.

70. Previous isotopic layering experiments with O_2 ESD from H_2O layers on Pt(111) have shown that all molecular oxygen is produced at/near the ASW/vacuum interface, but part of the O_2 precursors are produced at the Pt(111)/ASW interface and migrate through the film

71. G. A. Kimmel and T. M. Orlando, *Phys. Rev. Lett.*, 1996, **77**, 3983-3986.

72. G. A. Grieves and T. M. Orlando, *Surf. Sci.*, 2005, **593**, 180-186.

73. T. M. Orlando and M. T. Sieger, *Surf. Sci.*, 2003, **528**, 1-7.

74. A. Yabushita, T. Hama, D. Iida, N. Kawanaka, M. Kawasaki, N. Watanabe, M. N. R. Ashfold and H. P. Loock, *J. Chem. Phys.*, 2008, **129**, 044501.

75. A. Yabushita, Y. Hashikawa, A. Ikeda, M. Kawasaki and H. Tachikawa, *J. Chem. Phys.*, 2004, **120**, 5463-5468.

76. S. B. King, D. Wegkamp, C. Richter, M. Wolf and J. Stahler, *J. Phys. Chem. C*, 2017, **121**, 7379-7386.

77. C. Gahl, U. Bovensiepen, C. Frischkorn and M. Wolf, *Phys. Rev. Lett.*, 2002, **89**, 107402.

78. C. D. Lane, N. G. Petrik, T. M. Orlando and G. A. Kimmel, *J. Chem. Phys.*, 2007, **127**, 224706.

79. D. M. Chipman, *J. Chem. Phys.*, 2006, **124**, 044305.

80. D. M. Chipman, *J. Chem. Phys.*, 2005, **122**, 044111.

81. V. Engel, V. Staemmler, R. L. Vander Wal, F. F. Crim, R. J. Sension, B. Hudson, P. Andresen, S. Hennig, K. Weide and R. Schinke, *Journal of Physical Chemistry*, 1992, **96**, 3201-3213.

82. K. Kobayashi, *Journal of Physical Chemistry*, 1983, **87**, 4317-4321.

83. V. Y. Sukhonosov, *High Energy Chem.*, 1998, **32**, 71-76.

84. D. M. Bartels and R. A. Crowell, *J. Phys. Chem. A*, 2000, **104**, 3349-3355.

85. P. H. Hahn, W. G. Schmidt, K. Seino, M. Preuss, F. Bechstedt and J. Bernholc, *Phys. Rev. Lett.*, 2005, **94**, 037404.

86. W. Chen, X. F. Wu and R. Car, *Phys. Rev. Lett.*, 2010, **105**, 017802.

87. S. Suzuki, K. Fukui, H. Onishi and Y. Iwasawa, *Phys. Rev. Lett.*, 2000, **84**, 2156-2159.

88. M. Kunat, U. Burghaus and C. Woll, *Phys. Chem. Chem. Phys.*, 2004, **6**, 4203-4207.

89. R. Kramer and M. Andre, *J. Catal.*, 1979, **58**, 287-295.

90. P. Samson, A. Nesbitt, B. E. Koel and A. Hodgson, *J. Chem. Phys.*, 1998, **109**, 3255-3264.

91. M. R. Voss, H. Busse and B. E. Koel, *Surf. Sci.*, 1998, **414**, 330-340.

Graphical abstract

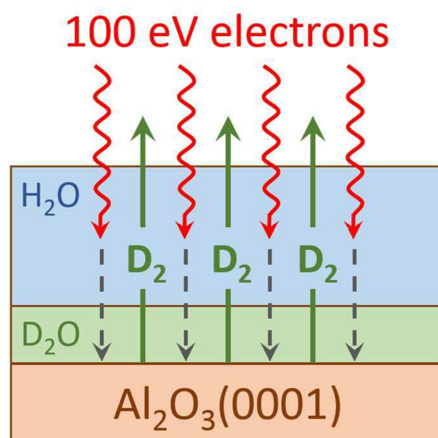

100 eV electrons are stopped in the H_2O portion of the isotopically-layered nanoscale film on α-$Al_2O_3(0001)$ but D_2 is produced at the D_2O/alumina interface by mobile electronic excitations and/or hydronium ions.

Graphical abstract

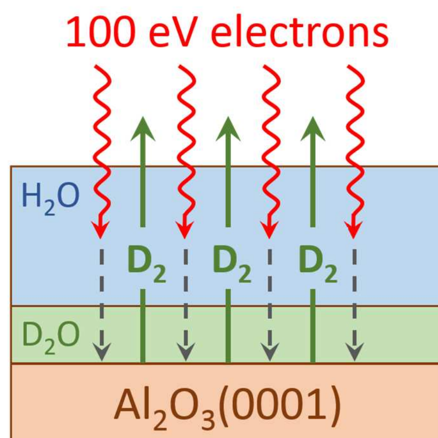

100 eV electrons are stopped in the H_2O portion of the isotopically-layered nanoscale film on α-Al_2O_3(0001) but D_2 is produced at the D_2O/alumina interface by mobile electronic excitations and/or hydronium ions.